iScience

CellPress
OPEN ACCESS

Article

Oncogenic HPV-induced high expression of ESM1 predicts poor prognosis and regulates aerobic glycolysis in cervical cancer

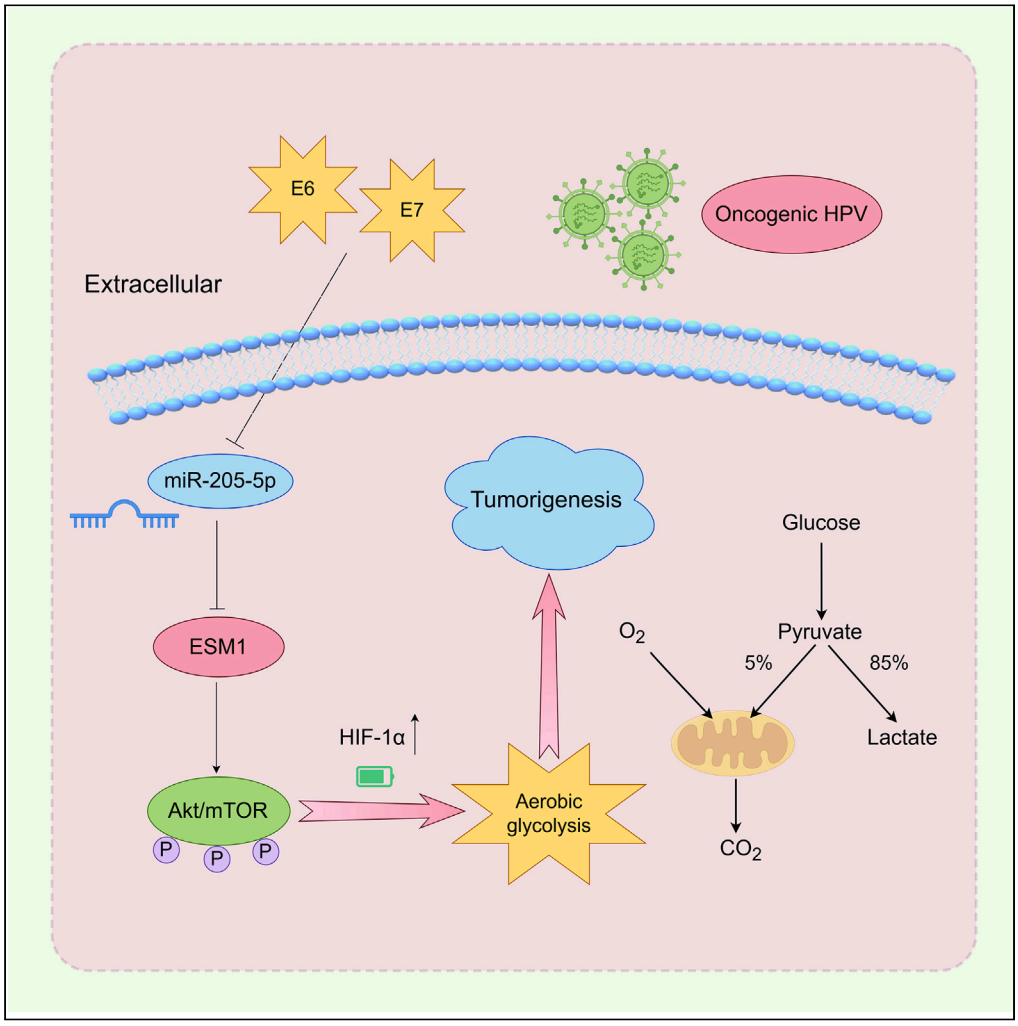

Lin Yuan, Yunqiu Wang, Mengyuan Yu, Zitong Feng, Ming Ci, Chunqing Wang, Hanxiang Chen

wangchunqing@sdfmu.edu.cn (C.W.)
hxchen@sdfmu.edu.cn (H.C.)

Highlights

ESM1 is highly expressed in CESC and can serve as an independent prognostic marker

Oncogenic HPV E6 and E7 upregulate ESM1 expression via the inhibition of miR-205-5p

ESM1 promotes aerobic glycolysis through the Akt/mTOR pathway

Yuan et al., iScience 27, 110112
June 21, 2024
https://doi.org/10.1016/j.isci.2024.110112

iScience

CellPress
OPEN ACCESS

Article

Oncogenic HPV-induced high expression of ESM1 predicts poor prognosis and regulates aerobic glycolysis in cervical cancer

Lin Yuan,[1,4] Yunqiu Wang,[1,4] Mengyuan Yu,[2] Zitong Feng,[3] Ming Ci,[1] Chunqing Wang,[1,*] and Hanxiang Chen[1,5,*]

SUMMARY

The impact of endothelial cell-specific molecule 1 (ESM1) on the initiation and progression of diverse cancers has been extensively studied, yet its regulatory mechanisms in relation to cervical cancer remain insufficiently understood. Through bioinformatics analysis, we revealed that ESM1 was highly expressed in cervical squamous cell carcinoma and endocervical adenocarcinoma (CESC) and correlated with dismal clinicopathological features. The activation of ESM1 is facilitated by the presence of oncogenic HPV E6 and E7. HPV E6 and E7 enhance the expression of ESM1 by diminishing the levels of miR-205-5p, which specifically targets the 3′ untranslated region of ESM1 mRNA. In addition, we demonstrated that ESM1 facilitates aerobic glycolysis of cervical cancer cells via the Akt/mTOR pathway. Suppression of ESM1 led to a reduction in the expression of HIF-1α and multiple glycolytic enzymes. Taken together, our findings provide insights into the mechanisms by which HPV infections regulate oncogenes, thereby contributing to cervical carcinogenesis.

INTRODUCTION

Cervical cancer is the fourth most common malignancy among women globally, with an estimated 604,000 new cases and 342,000 new deaths in 2020.[1] More than 90% of cervical cancer cases are associated with certain oncogenic HPV types, especially HPV 16 and 18.[2] Most HPV infections can be cleared spontaneously within months by the immune system, but 10–15% persistently exist, consequently promoting the progression of precancerous cervical intraepithelial neoplasia (CIN) to invasive cervical carcinoma.[3] Despite preventive vaccines and early diagnosis, which have reduced mortality in recent years, the 5-year survival rate of patients with advanced cervical cancer remains unsatisfactory.[4] The rapid development of molecular targeted therapy has provided more choices for cervical cancer treatment; however, existing biomarkers are far from sufficient, and there is still a requirement to explore more efficient biomarkers and innovative therapies to improve the prognosis of patients with cervical cancer.

Endothelial cell-specific molecule 1 (ESM1), also known as endocan, is a soluble dermatan sulfate proteoglycan released by vascular endothelial cells in several organs, mainly the lungs and kidneys.[5] ESM1 plays an important role in regulating cell adhesion, inflammatory cytokines, angiogenesis, vascular disorders, lymphocyte functions, and endothelial cytoskeleton rearrangement.[6–8] Misregulation of ESM1 expression is associated with many human diseases such as hypertension, intermittent hypoxia, chronic renal failure, and human tumors.[9] Overexpression of ESM1 in triple-negative breast cancer promotes cell proliferation by activating the Akt-dependent NF-κB/cyclin D1 pathway.[10] ESM1 regulates cell growth and metastasis by activating NF-κB in colorectal cancer.[11] A survival prediction model was constructed in the context of cervical cancer by integrating ESM1 and five additional genes that are linked to hypoxia and angiogenesis.[12] The overexpression of ESM1 has been found to facilitate carcinoma angiogenesis and the progression of cervical cancer via the VEGF/ERK signaling pathway.[13] Despite the carcinogenic role of ESM1 in cervical cancer is emerging, a comprehensive understanding of its involvement and regulatory mechanism in the initiation and progression of cervical cancer, as well as its correlation with HPV infection, has not been fully elucidated.

In this report, we identified that ESM1 was markedly overexpressed in cervical squamous cell carcinoma and endocervical adenocarcinoma (CESC) using The Cancer Genome Atlas (TCGA) and Genotype-Tissue Expression (GTEx) databases. High ESM1 expression exhibited diagnostic and prognostic value in patients with CESC. Aberrant expression of ESM1 was demonstrated to be regulated by oncogenic HPV E6 and E7 by reducing miR-205-5p expression. In addition, we found that ESM1 might exert its carcinogenic function by regulating aerobic glycolysis through the activation of the Akt/mTOR signaling pathway.

[1]Department of Clinical Laboratory Medicine, The First Affiliated Hospital of Shandong First Medical University & Shandong Provincial Qianfoshan Hospital, Shandong Medicine and Health Key Laboratory of Laboratory Medicine, Jinan, Shandong, P.R. China
[2]Department of Radiation Oncology, the Third Hospital Affiliated with Shandong First Medical University, Jinan, Shandong, P.R. China
[3]Department of Thoracic Surgery, Qilu Hospital, Cheeloo College of Medicine, Shandong University, Jinan, Shandong, P.R. China
[4]These authors contributed equally
[5]Lead contact
*Correspondence: wangchunqing@sdfmu.edu.cn (C.W.), hxchen@sdfmu.edu.cn (H.C.)
https://doi.org/10.1016/j.isci.2024.110112

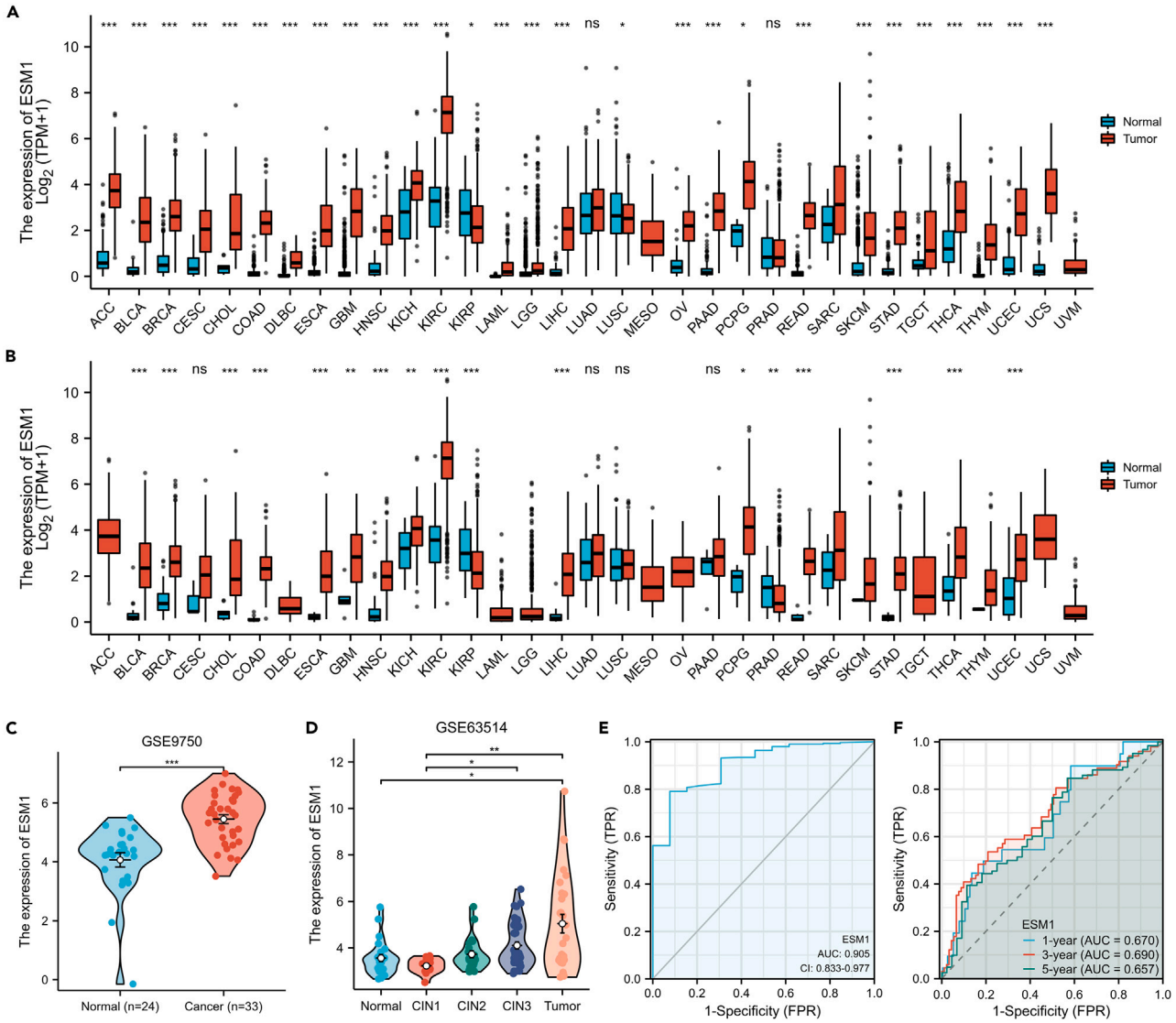

Figure 1. The expression of ESM1 is aberrantly increased in CESC

(A and B) Boxplots assessing the expression profiles of ESM1 between tumor and normal tissue (A) or between tumor and pericarcinous tissue (B) in different types of cancers based on the TCGA and GTEx datasets. The x axis abbreviations represent tumor types.

(C) The validation of ESM1 expression in GSE9750 dataset.

(D) The expression difference of ESM1 in normal tissue (n = 24), CIN1 (n = 14), CIN2 (n = 22), CIN3 (n = 40) and tumor tissue (n = 28), from GSE63514 dataset.

(E) Receiver operating characteristic (ROC) curve analysis evaluating the performance of ESM1 for CESC diagnosis.

(F) The predictive accuracy of ESM1 was reflected by time-dependent ROC analysis with AUC of the 1st, 3rd and 5th years. *$p < 0.05$, **$p < 0.01$, and ***$p < 0.001$.

RESULTS

ESM1 is upregulated in cervical squamous cell carcinoma and endocervical adenocarcinoma

We examined the expression of ESM1 using pan-cancer analysis. As shown in Figure 1A, based on the TCGA and GTEx databases, ESM1 was upregulated in 26 out of 33 cancer types compared with normal tissues, including CESC. Meanwhile, compared with cancer-adjacent normal tissues, ESM1 displayed a significantly elevated expression level across multiple cancer types (Figure 1B). The expression of ESM1 was additionally confirmed in the GSE9750 dataset (Figure 1C). In the GSE63514 dataset, ESM1 exhibited upregulation in tumors relative to CIN, and a statistically significant distinction was observed between CIN1 and CIN3 (Figure 1D). To better understand the prognostic role of ESM1 in CESC, we performed ROC curve analysis based on the TCGA dataset. ESM1 showed high sensitivity and specificity (AUC = 0.905) for CESC diagnosis (Figure 1E). The prediction capacity of ESM1 was also assessed by time-dependent ROC analysis (Figure 1F). These results suggest that ESM1 exhibits elevated expression levels in cervical cancer tissues and may possess diagnostic value.

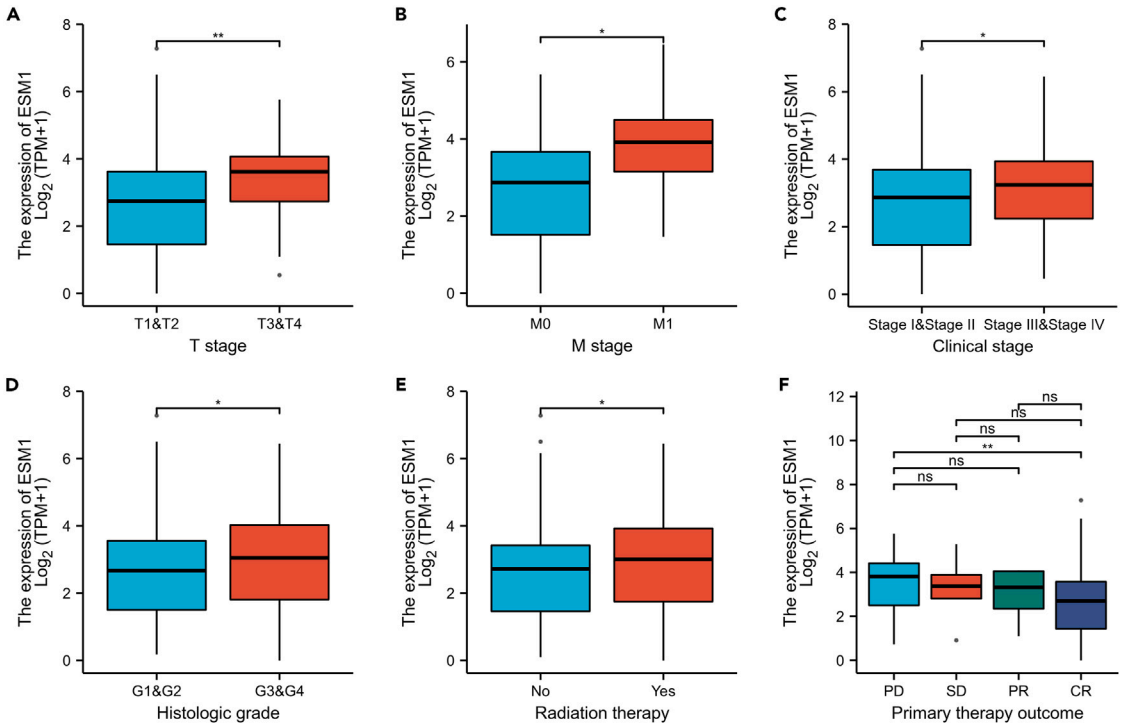

Figure 2. The expression of ESM1 is associated with various clinical characteristics in CESC based on data from the TCGA

(A) T stage; (B) M stage; (C) Clinical stage; (D) Histologic grade; (E) Radiation therapy; (F) Primary therapy outcome. PD, progressive disease; SD, stable disease; PR, partial response; CR, complete response. *$p < 0.05$, **$p < 0.01$.

Association of ESM1 expression and clinicopathological variables in CESC

In order to elucidate the role and importance of ESM1 in cervical cancer, we conducted an analysis to examine the correlation between the expression of ESM1 and clinicopathological parameters in patients diagnosed with CESC using the TCGA dataset. As shown in Figures 2A–2E, the high expression of ESM1 was significantly correlated with T stage (T3 and 4 vs. T1 and 2), M stage (M1 vs. M0), clinical stage (stage III and IV vs. stage I and II), histologic grade (G3 and 4 vs. G1 and 2), and radiation therapy (yes vs. no). In addition, the expression level of ESM1 was significantly different between progressive disease (PD) group and complete response (CR) groups in CESC patients (Figure 2F). As shown in Table 1, the results of the univariate analysis using logistic regression also indicated that ESM1 expression was correlated with poor prognostic clinical characteristics in CESC patients, including T stage (OR = 1.440, $p = 0.009$), M stage (OR = 1.884, $p = 0.012$), clinical stage (OR = 1.216, $p = 0.048$), and primary therapy outcome (OR = 0.638, $p = 0.002$). The findings indicate that the expression of ESM1 is correlated with clinical characteristics in CESC.

High expression of ESM1 is an independent prognostic indicator to CESC

Next, the prognostic significance of ESM1 was assessed by Kaplan–Meier analysis. As shown in Figures 3A–3C, the increased expression of ESM1 predicted poor prognosis in terms of overall survival (OS, HR:1.93, $p = 0.007$), disease-specific survival (DSS, HR:2.03, $p = 0.012$), and progression-free interval (PFI; HR:1.71, $p = 0.026$). Univariate and multivariate analysis using the Cox proportional hazards regression model were conducted based on the TCGA dataset. As shown in Table 2, the univariate Cox regression analysis revealed that clinical T, N, and M stages, clinical stages, and ESM1 were positive prognostic factors indicating worsen CESC patient overall survival. In multivariate regression Cox analysis, T, N, clinical stages, and ESM1 were independent risk factors for overall survival in CESC.

Subsequently, a nomogram was constructed considering the statistically significant prognostic factors in the multivariate Cox regression analysis to predict 3, five and 7-year overall survival of CESC (Figure 3D). The sum of the points assigned to each parameter was readjusted to a range of 1–100. The calibration plots showed a good agreement between the predicted and observed events (Figure 3E). When survival analysis was orchestrated in CESC subgroups, the upregulated ESM1 also predicted poor prognosis, particularly in cases with age $\leq$50, squamous cell carcinoma, and histologic grade 3 (Figure 3F). The above results illustrate that high expression of ESM1 serves as an independent risk factor for predicting an unfavorable prognosis in CESC.

High-risk HPV infection induces the up-regulation of ESM1 primarily by oncoprotein E6 and E7

In order to investigate the involvement of ESM1 in cervical cancer, we confirmed the upregulation of ESM1 both *in vivo* and *in vitro*. Compared with normal cervical tissues, the mRNA and protein levels of ESM1 were increased in cervical cancer tissues (Figures 4A and 4B). In addition, we

Table 1. Logistic regression analysis of association between ESM1 expression and clinicopathological characteristics in CESC patients

Characteristics	Total(N)	Odds Ratio(OR)	*p* value
T stage (T3&T4 vs. T1&T2)	243	1.440 (1.100–1.903)	**0.009****
N stage (N1 vs. N0)	195	0.962 (0.773–1.190)	0.722
M stage (M1 vs. M0)	127	1.884 (1.178–3.220)	**0.012***
Clinical stage (Stage III&Stage IV vs. Stage I&Stage II)	299	1.216 (1.003–1.480)	**0.048***
Radiation therapy (Yes vs. No)	306	1.173 (0.994–1.390)	0.062
Primary therapy outcome (PR&CR vs. PD&SD)	219	0.638 (0.473–0.845)	**0.002****

*$p<0.05$, **$p<0.01$.

observed a significant upregulation of ESM1 expression in the serum of cervical cancer patients compared to a healthy control group (Figure 4C). The elevated level of ESM1 was associated with a poorer overall survival in a cohort of 69 cervical cancer patients (Figure 4D). Further, we examined the mRNA and protein expression levels of ESM1 in cervical cancer cell lines HeLa, SiHa, CaSki, C33A, and the immortalized cervical epithelial cell line H8 (HeLa, SiHa, CaSki and H8 are HPV positive, C33A is HPV negative). As shown in Figure 4E, ESM1 was increased in HeLa and SiHa cells. Similarly, compared with C33A cells, ESM1 expression was upregulated in HeLa and SiHa cells at the protein level (Figure 4F).

Given that the E6 and E7 proteins of only the high-risk HPVs are responsible for oncogenic transformation of HPV-infected cells, we investigated the effect of E6 and E7 on ESM1 expression. The expression of ESM1 was significantly increased in HPV E6/E7-expressing RPE1 cells (Figures 4G and 4H). Overexpression of HPV E6/E7 also leads to an increase in the protein levels of ESM1 in HeLa and SiHa cells (Figure S1). Additionally, siRNA targeting HPV18 E6/18 E7 or 16 E6/16 E7 significantly decreased ESM1 expression in HPV18-positive HeLa or HPV16-positive SiHa cells at both mRNA (Figures 4I and 4K) and protein levels (Figures 4J and 4L). Owing to HPV E6 and E7 proteins are unstable and not easily detected, the expression of p53 (a target of E6) and pRb (a target of E7) was used to prove knockdown efficiency. These data illustrate that the aberrant expression of ESM1 in cervical cancer is caused by the HPV E6 and E7 oncoproteins.

HPV infection promotes ESM1 expression by inhibition of miR-205a-5p production

MicroRNAs (miRNAs) play diverse roles in various physiological processes. Aberrant expression of multiple miRNAs has been observed in cervical cancer, with many being regulated by HPV.[14] In order to uncover the mechanisms resulting in the increased expression of ESM1 in cervical cancer, we sought to investigate whether miRNAs were implicated in this process. A total of 105 miRNAs that were downregulated in cervical cancer, as summarized in the literature,[15] were chosen for analysis. The analysis involved utilizing a Venn diagram to compare these miRNAs with the predicted ESM1 upstream miRNAs obtained from miRDB and Targetscan databases. As shown in Figure 5A, miR-22-5p, miR-205-5p, and miR-4262 were intersected miRNAs, which were downregulated in cervical cancer tissues and had a consensus seed match in the ESM1 3′ UTR.

We verified the miRNA expression in HPV16 E6-and E7-expressing cells. As shown in Figure 5B, only miR-205-5p expression decreased in both E6-and E7-expressing cells. Knockdown of HPV18 E6/18 E7 or 16 E6/16 E7 in HeLa and SiHa cells significantly increased the expression of miR-205-5p (Figure 5C). Next, we examined the effect of miR-205-5p on ESM1 expression in HeLa and SiHa cells. As shown in Figure 5D, blocking miR-205-5p activity in HeLa and SiHa cells via transfection with an inhibitor increased ESM1 expression. Conversely, overexpression of miR-205-5p by transfection with miR-205-5p mimics decreased ESM1 expression (Figure 5E). The diagnostic performance of miR-205-5p was assessed using ROC analysis. The area under the curve (AUC) was 0.975, indicating high sensitivity and specificity for CESC diagnosis (Figure 5F).

To obtain more definitive evidence, luciferase reporters were constructed to contain the ESM1 3′-UTR with or without mutations that disrupt the miR-205-5p seed match (Figure 5G). Luciferase activity was determined and normalized to that of HEK293T cells. As shown in Figure 5H, miR-205-5p mimics showed strong inhibition of luciferase activity only when the reporter contained the WT 3′-UTR of ESM1. No inhibition was observed when the reporter contained the mutated 3′-UTR of ESM1. These results provide strong evidence that miR-205-5p downregulates ESM1 expression through a seed match in the ESM1 3′-UTR, ESM1 is a target of miR-205-5p in cervical cancer.

ESM1 accelerates glycolysis in cervical cancer

To further explore the underlying function and molecular pathways of the ESM1 gene in CESC, the differentially expressed genes (DEGs) of ESM1 based on the TCGA dataset were analyzed and displayed in volcano plots (Figure 6A). A total of 550 genes related to ESM1 expression were altered (396 upregulated, 154 downregulated, |log2(FC)| >1 & p. adj<0.05), which may reflect the potential value of ESM1 in CESC pathogenesis.

Subsequently, the GO and KEGG functional enrichment analysis was conducted using the DEGs of ESM1 in CESC (Figures 6B and 6C). KEGG analysis showed that the DEGs were enriched in ERK1 and ERK2 cascade, PI3K/Akt signaling pathway and cell metabolism. Using the high- and low- ESM1 expression datasets, we performed GESA to identify the most significantly altered pathways based on the gene sets from MSigDB (c2.cp.kegg.v6.2.symbols.gmt). The ridge plot showed that the DEGs of ESM1 were mostly involved in pathways in cancer,

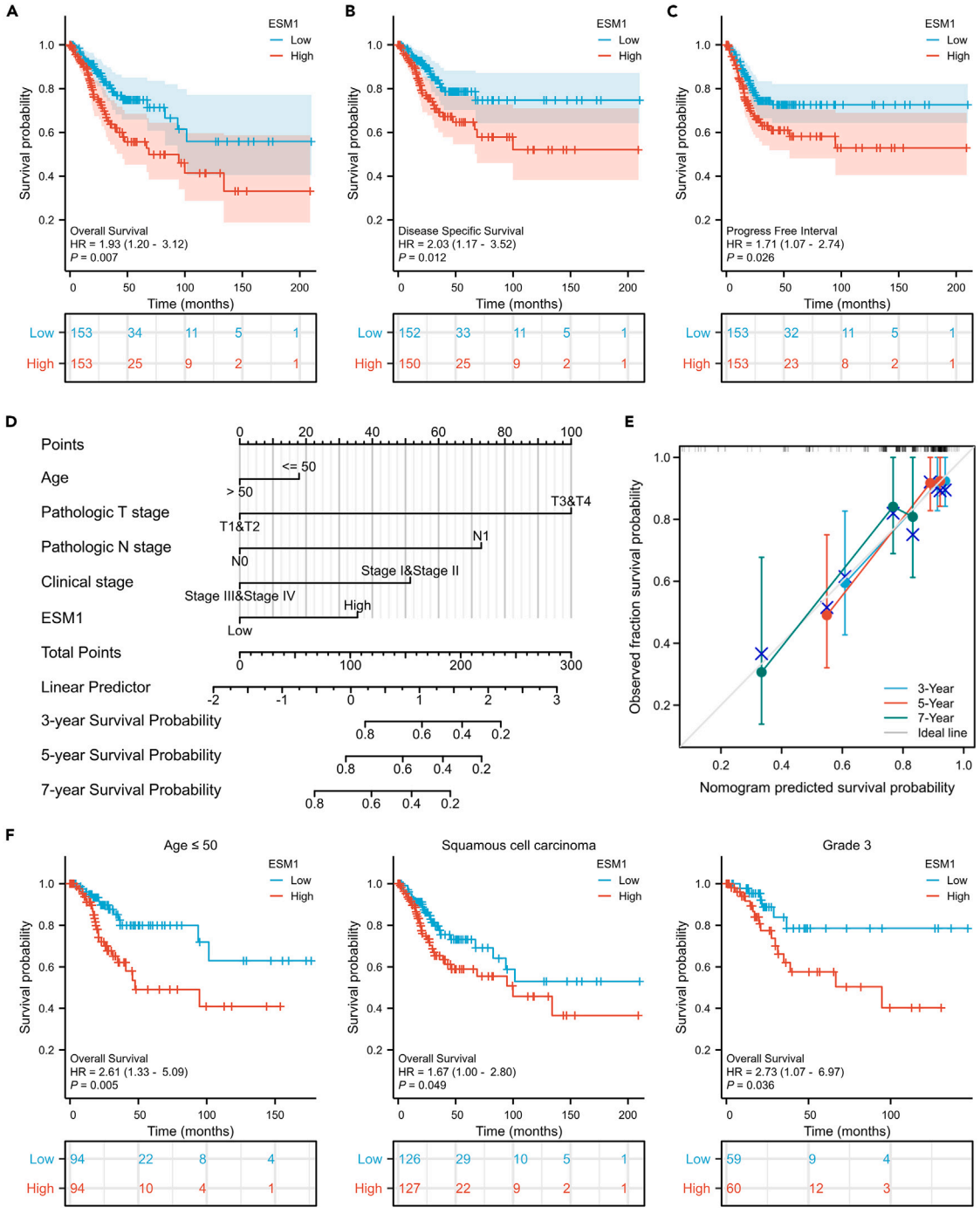

Figure 3. Prognostic value of ESM1 in CESC based on the TCGA database

(A–C) Kaplan-Meier analysis comparing overall survival (A), disease-specific survival (B), and progression-free interval (C) between low- and high-ESM1 expression groups.

(D) A nomogram for predicting probability of patients with 3-, 5- and 7-year overall survival.

(E) Calibration plots validating the efficiency of nomograms for overall survival.

(F) The prognostic values of ESM1 in different CESC subgroups.

Table 2. Cox regression analysis for clinical outcomes in CESC patient

		Univariate analysis		Multivariate analysis	
Characteristics	Total(N)	Hazard ratio (95% CI)	*p* value	Hazard ratio (95% CI)	*p* value
Age	306				
≤50	188	Reference			
>50	118	1.289 (0.810–2.050)	0.284		
T stage	243				
T1	140	Reference			
T2	72	1.152 (0.562–2.359)	0.700	0.000 (0.000-Inf)	0.993
T3	21	2.710 (1.167–6.292)	**0.020***	1.392 (0.175–11.053)	0.754
T4	10	8.088 (3.419–19.135)	**<0.001*****	1202277.463 (97718.564–14792185.156)	**<0.001*****
N stage	195				
N0	134	Reference			
N1	61	2.844 (1.446–5.593)	**0.002****	2.738 (1.003–7.477)	**0.049***
M stage	127				
M0	116	Reference			
M1	11	3.555 (1.187–10.641)	**0.023***	219.646 (0.000-Inf)	0.999
Clinical stage	299				
Stage I	162	Reference			
Stage II	69	0.813 (0.413–1.600)	0.548	0.000 (0.000-Inf)	0.993
Stage III	46	1.390 (0.707–2.734)	0.340	0.000 (0.000-Inf)	0.993
Stage IV	22	4.376 (2.354–8.137)	**<0.001*****	0.000 (0.000–0.001)	**<0.001*****
ESM1	306	1.534 (1.261–1.867)	**<0.001*****	1.816 (1.067–3.088)	**0.028***

CI, confidence interval.
**p*<0.05, ***p*<0.01, ****p*<0.0001.

signaling by receptor tyrosine kinases, MAPK family signaling cascades, and the PI3K/Akt signaling pathway, with a threshold of NES>1.5 and p. adj<0.05 (Figure 6D).

Studies have demonstrated that ESM1 can regulate the PI3K/Akt pathway in cervical cancer, which is in accordance with our bioinformatics analysis results.[16] HPV infection also influences the Akt/mTOR pathway in cervical cancer.[17,18] Our study confirmed its regulatory effects on glucose metabolism in RPE1 E6/E7 overexpressing cells (Figure S2). However, the effect of ESM1 on an important tumor survival strategy, the aerobic glycolysis, remains to be comprehensively understood. Given that the DEGs associated with ESM1 were found to be enriched in pathways related to tumorigenesis, it is plausible to hypothesize that ESM1 may exert an influence on glycolysis, thereby potentially facilitating the survival and proliferation of cervical cancer cells through direct or indirect mechanisms.

Based on the glycolysis-related prognostic risk score model developed by Cai et al., we conducted an analysis to examine the association between ESM1 and six predictive signatures.[19] Our findings, as depicted in Figure 6E, demonstrate a positive correlation between the expression of ESM1 and the risk factors HSPA5, ANGPTL4, PFKM, IER3, and PFKFB4 ($p < 0.001$), which have been linked to glycolysis and are indicative of poor survival outcomes in cervical cancer. Conversely, we observed a negative correlation between ESM1 expression and the protective factor GOT1 ($p < 0.05$). Furthermore, our analysis of the TCGA dataset revealed a significant association between ESM1 expression and several key glycolytic enzymes in CESC (Figure 6F).

Next, the role of ESM1 in glycolysis was examined in cervical cancer HeLa and SiHa cells. ESM1 knockdown was achieved through RNA interference, whereas ESM1 overexpression was accomplished via transfection of cells with the pENTER-hESM1 plasmid. The efficacy of these interventions was assessed using RT-qPCR and immunoblotting techniques, respectively (Figures 6G and 6H). HeLa-siESM1 and SiHa-siESM1 cells showed a significant reduction in cell viability compared with control cells after siRNA transfection (Figure 6I). Knockdown of ESM1 led to a notable decrease in the relative glucose uptake, lactate production and intracellular ATP levels. Conversely, the upregulation of ESM1 resulted in heightened glucose uptake, lactate production and intracellular ATP levels in HeLa and SiHa cells compared with normal control cells (Figures 6J–6L). Taken together, these data imply that ESM1 may accelerate glycolysis in cervical cancer cells.

ESM1 regulates glycolysis in cervical cancer partially via activating the Akt/mTOR pathway

Among the DEGs enriched pathways, the Akt/mTOR pathway has been demonstrated to promote aerobic glycolysis in tumor cells by regulating glucose transporters and glycolytic enzymes on the cell surface. However, the extent to which the involvement of ESM1 contributes to

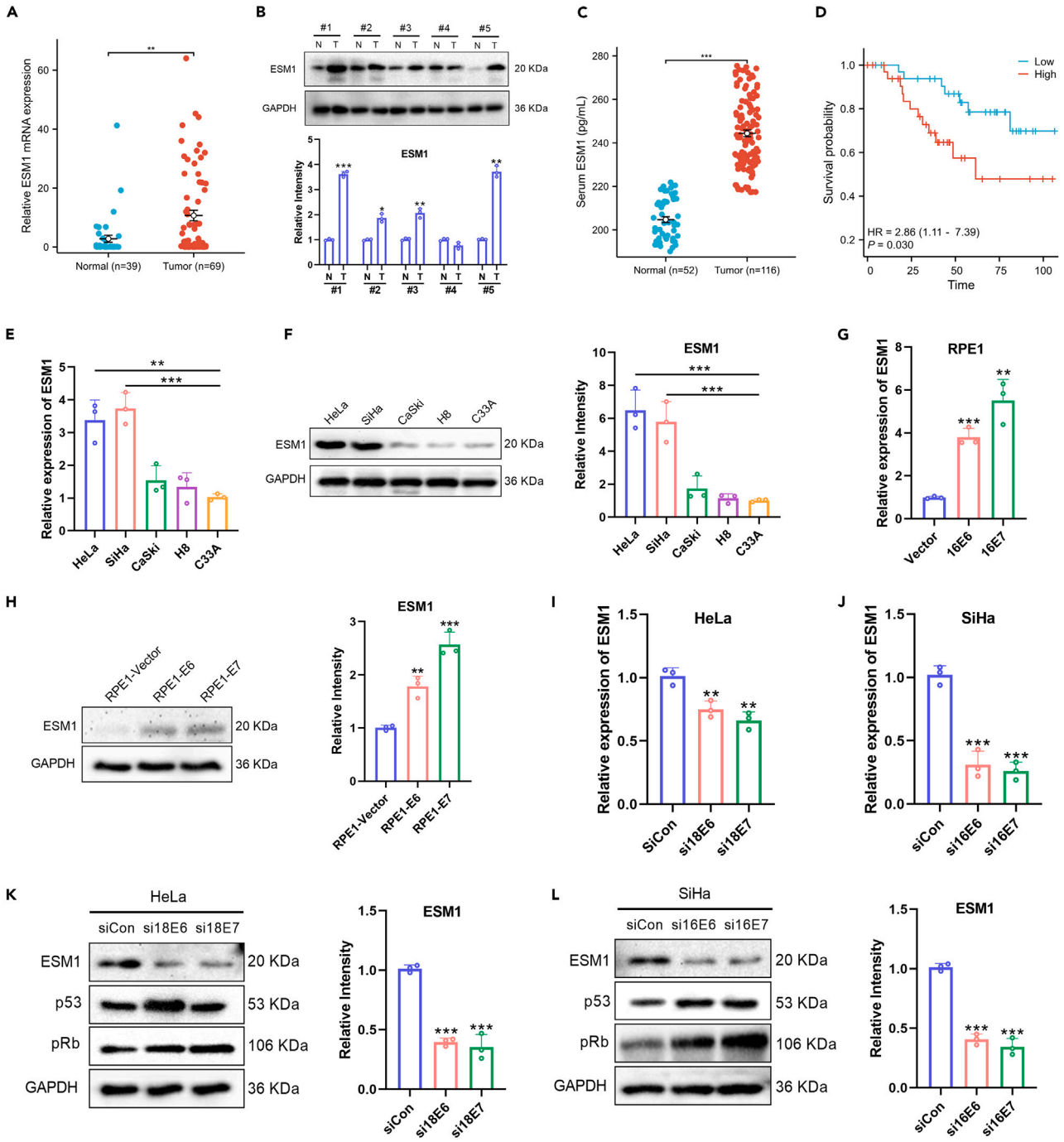

Figure 4. Virus oncoproteins E6 and E7 regulate the expression of ESM1 in cervical cancer cells

(A) RT-qPCR analysis of the mRNA expression of ESM1 in non-cancer cervical tissues (n = 39) and cervical cancer tissues (n = 69).

(B) Representative immunoblotting images on the protein levels of ESM1 in 5 paired of cervical cancer tissues and normal cervical tissues.

(C) Levels of ESM1 in serum of healthy controls (n = 52) and cervical cancer patients (n = 116) measured by ELISA.

(D) Kaplan-Meier curves for overall survival of 69 patients with cervical cancer according to ESM1 expression.

(E) RT-qPCR analysis of relative mRNA level of ESM1 in cervical cancer cell lines (HeLa, SiHa, CaSki, H8 and C33A).

(F) Immunoblotting analysis of ESM1 expression in cervical cancer cell lines.

(G and H) RT-qPCR analysis and immunoblotting analysis of ESM1 in HPV16 E6-and E7-expressing RPE1 cells were shown. Detection of ESM1 mRNA level and protein level of ESM1 in HeLa cells (I, K) and SiHa cells (J, L) after transfection with siRNAs targeting HPV18 E6, 18 E7 or 16 E6, 16 E7. The protein level of p53 and pRb were examined to evaluate the transfection efficiency of siE6 and siE7, respectively. Data are shown as mean ± SD of three independent experiments (*$p < 0.05$, **$p < 0.01$, and ***$p < 0.001$).

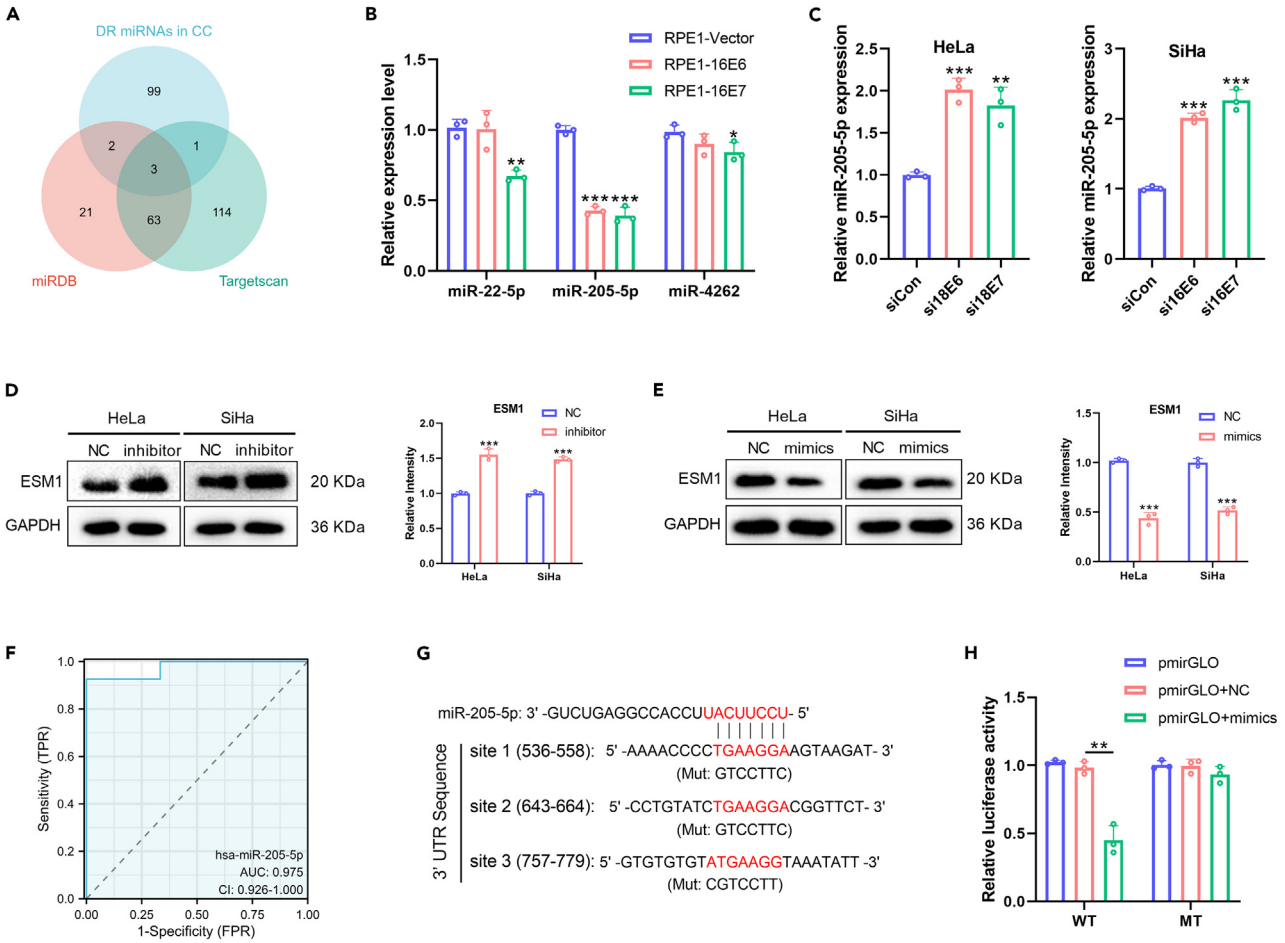

Figure 5. miR-205-5p targets the 3′ UTR of ESM1 and reduces ESM1 protein expression

(A) Venn diagram showing the overlap of miRNAs among downregulated miRNAs by HPV, and the predicted miRNAs with consensus seed match in the ESM1 3′ UTR. The three intersected miRNAs are miR-22-5p, miR-205-5p and miR-4262. DR: downregulated; CC: cervical cancer.

(B) RT-qPCR analysis of miR-22-5p, miR-205-5p and miR-4262 expression in HPV16 E6-and E7-expressing RPE1 cells.

(C) RT-qPCR analysis of miR-205-5p expression in HeLa and SiHa cells transfected with siE6 or siE7.

(D and E) Immunoblotting analysis of ESM1 in HeLa and SiHa cells transfected with miR-205-5p inhibitor or mimics.

(F) ROC curve analysis evaluating the performance of miR-205-5p for CESC diagnosis based on the TCGA database. (G) Predicted and mutant sequence alignment of miR-205-5p target sites in the ESM1 3′ UTR.

(H) The wild-type (WT) or mutant (MT) reporter of ESM1 was cotransfected with control or miR-205-5p mimics into HEK293T cells, the dual luciferase activity was determined at 48 h posttransfection. Data are shown as mean ± SD of three independent experiments (*$p < 0.05$, **$p < 0.01$, and ***$p < 0.001$).

glycolysis in cervical cancer, specifically in relation to the reliance on this metabolic pathway, remains undisclosed. Immunoblotting analysis showed that the inhibition of ESM1 resulted in a decrease in the levels of *p*-Akt, *p*-mTOR, and HIF-1α. Conversely, the overexpression of ESM1 was found to activate the Akt/mTOR pathway in HeLa and SiHa cells (Figure 7A). The expression of ESM1 was positively correlated with HIF-1α in CESC based on the TCGA dataset (Figure 7B). More intriguingly, the findings presented in Figure 7C indicate that the downregulation of ESM1 in HeLa and SiHa cells led to a reduction in the expression levels of diverse glycolytic enzymes, which is consistent with the results obtained from bioinformatics analysis (Figure 6F).

By using the PI3K/Akt pathway inhibitor LY294002, we found the relative glucose uptake, lactate production and intracellular ATP levels were significantly decreased in ESM1 overexpression HeLa or SiHa cells (Figures 7F–7H). The inhibitory effect of LY294002 on PI3K phosphorylation was examined by immunoblotting (Figure 7D). LY294002 had no effect on ESM1 expression (Figure 7E). The graphical representation in Figure 7I provides a summary of the interactional model of molecules and the potential mechanism of ESM1 in the regulation of cervical cancer tumorigenesis.

DISCUSSION

Despite remarkable advancements in HPV vaccines, cervical cancer remains a major threat to women globally, particularly in developing or least-developed countries. Clinical staging for cervical cancer was based on the International Federation of Gynecology and Obstetrics

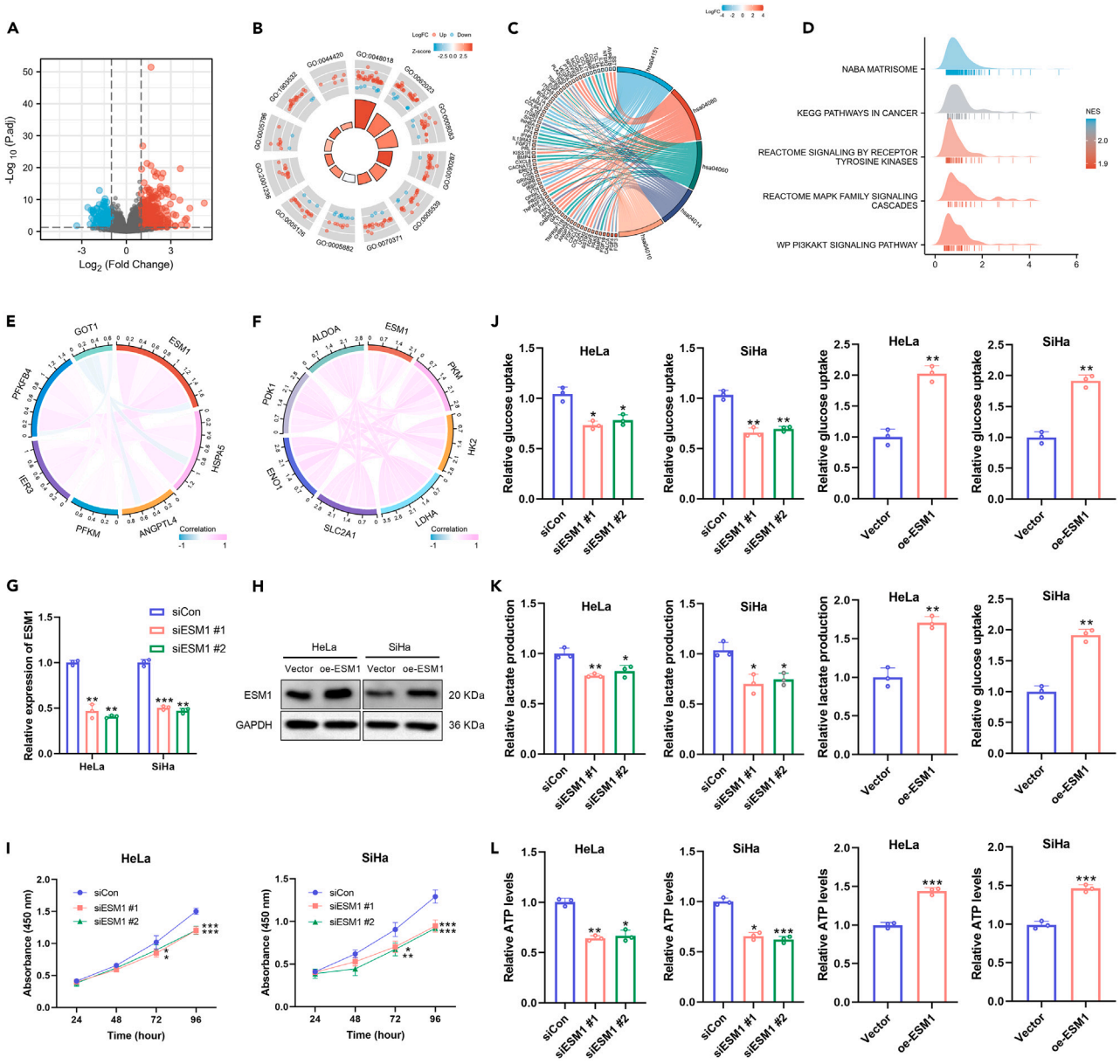

Figure 6. ESM1 promotes aerobic glycolysis of cervical cancer cells *in vitro*

(A) Volcano plot depicting the ESM1-correlated DEGs.

(B) Ridge plot of significantly enriched pathways with the threshold of NES>1.5 and p. adj<0.05.

(C) The functional enrichment results by ESM1-correlated DEGs in terms of biological processes, molecular functions and cellular components.

(D) Chord diagram of enriched KEGG signaling pathways. Gene patches (left) correspond to different log_2FC values, Entry patches (right) with different size represent the different number of molecules contained.

(E) Correlation analysis from the TCGA database between ESM1 and six genes associated with glycolysis which can predict poor survival of cervical cancer.

(F) Correlation between ESM1 and glycolytic enzyme expression in CESC from the TCGA database.

(G) The knockdown efficiency of siESM1 was assessed through RT-qPCR analysis.

(H) The ESM1 expression plasmid was transfected into HeLa and SiHa cells, and subsequently evaluated via Immunoblotting.

(I) CCK-8 assay of HeLa and SiHa cells transfected with ESM1 siRNA.

(J–L) Glucose uptake (J), lactate production (K) and intracellular ATP levels (L) in HeLa and SiHa cells transfected with ESM1 siRNA or an overexpression plasmid was analyzed. Data are shown as mean ± SD of three independent experiments (*$p < 0.05$, **$p < 0.01$, and ***$p < 0.001$).

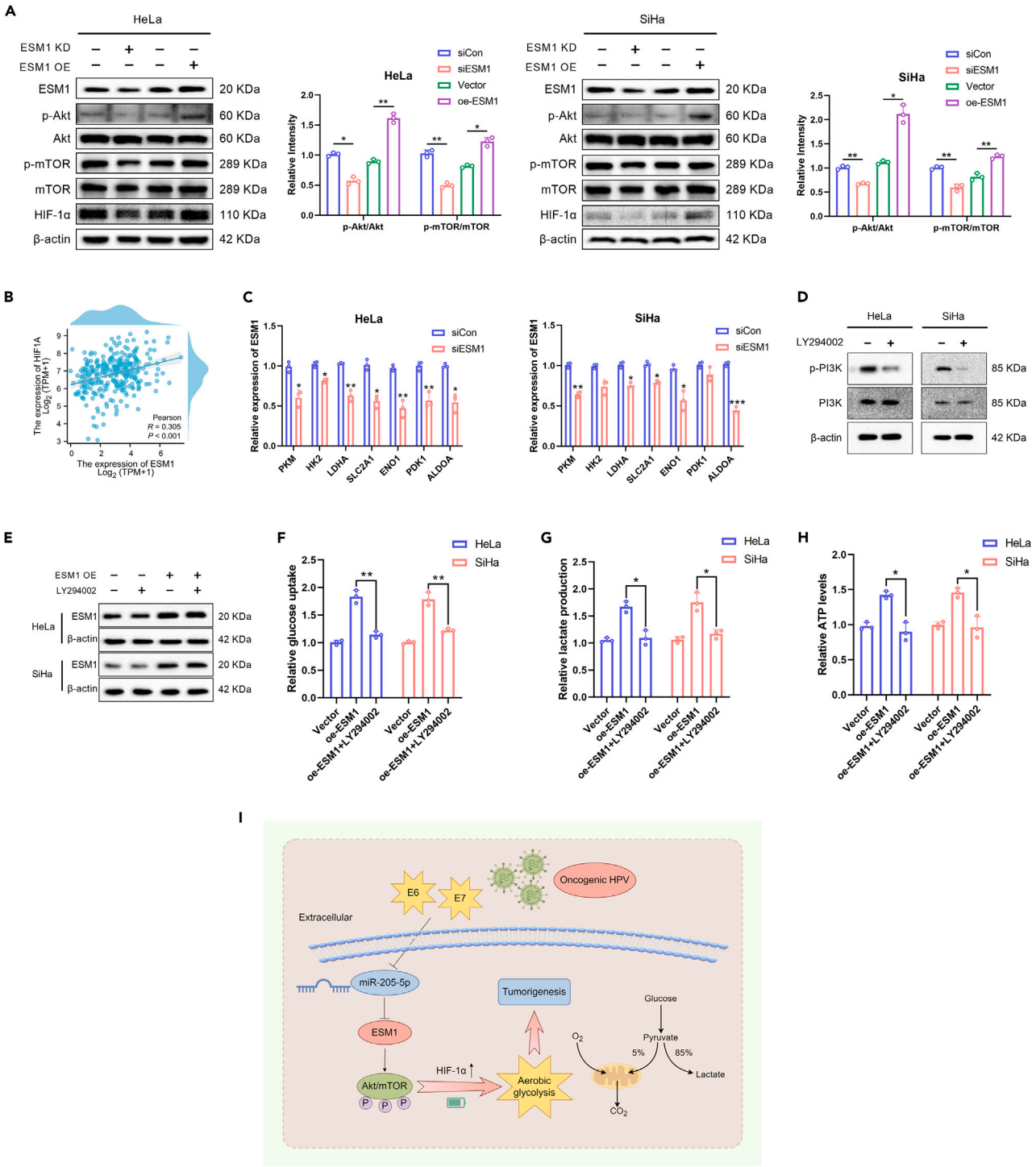

Figure 7. ESM1 regulates aerobic glycolysis of cervical cancer cells partially by activating Akt/mTOR pathway

(A) Akt, *p*-Akt, mTOR, *p*-mTOR and HIF-1α proteins were detected by Immunoblotting in HeLa and SiHa cells with the applied genetic modifications. KD: knockdown; OE: overexpression.

(B) The correlation between the expression of ESM1 and HIF-1α in CESC based on the TCGA dataset.

(C) RT-qPCR analysis of relative mRNA level of PKM, HK2, LDHA, SLC2A1, ENO1, PDK1 and ALDOA in HeLa and SiHa cells transfected with ESM1 siRNA.

(D) PI3K and p-PI3K proteins were detected by Immunoblotting in HeLa and SiHa cells treated with 20 μM LY294002 for 24h.

Figure 7. *Continued*

(E) Immunoblotting analysis of ESM1 in HeLa and SiHa cells treated with LY294002. Glucose uptake (F), lactate production (G) and intracellular ATP levels (H) in HeLa and SiHa cells transfected with vector, ESM1, or ESM1+LY294002.

(I) Proposed model of ESM1-mediated aerobic glycolysis in oncogenic HPV-induced cervical cancer. Data are shown as mean ± SD of three independent experiments (*$p < 0.05$, **$p < 0.01$, and ***$p < 0.001$).

(FIGO) system.[20] However, it is common for the survival of cervical cancer patients to differ significantly within the same FIGO staging, suggesting that more effective prognostic markers are required to personalize risk assessment and help develop specific treatment plans.

Using bioinformatics tools, we previously screened potential prognostic biomarkers for CESC based on the TCGA and GTEx databases. Notably, ESM1 was significantly upregulated in CESC and associated with overall survival. Upregulated ESM1 was correlated with CIN levels and clinicopathological variables such as T, M, clinical stages, and primary therapy outcomes. Using ROC curve analysis, ESM1 was confirmed as a potential marker for the diagnosis of CESC with high sensitivity and specificity. Multivariate Cox analysis further confirmed that high ESM1 expression is an independent risk factor for OS in patients with CESC.

Emerging evidence suggests that ESM1 may participate in the occurrence and development of human cancers. For instance, high ESM1 expression contributes to cell proliferation and migration in head and neck cancer cells.[21] In adrenocortical carcinoma cells, overexpression of ESM1 upregulated CDK1 and p21-mediated G2/M-phase transition, cell proliferation, cell migration, cell invasion, and accumulation of tumor mutation burden via DLL4-Notch signaling pathway.[22] Although the role of ESM1 in human carcinomas has gradually been revealed, the function and potential mechanisms of ESM1 in cervical cancer are still lacking. One study demonstrated that ESM1 drives cervical cancer cell proliferation, cell cycle progression, and *in vitro* cell migration and invasion by targeting SYT13, followed by activation of the PI3K-Akt pathway.[16] However, the etiology behind the heightened levels of ESM1 in cervical cancer and its involvement in tumor cell metabolism remains elusive. The relationship between the aberrant expression of ESM1 and HPV infection is also unclear, which piques our interest for further exploration.

In order to authenticate the findings of the bioinformatics analysis, we conducted assessments of ESM1 levels *in vivo* and *in vitro* settings. Notably, ESM1 demonstrated elevated expression levels in both cervical cancer tissues and patient sera in comparison to control samples. More importantly, ESM1 was upregulated in RPE1 cells stably expressing HPV 16E6 or 16E7, and knockdown of HPV 18E6/E7 or HPV 16E6/E7 in HeLa and SiHa cells significantly attenuated the expression of ESM1. The E6-specific siRNA (siE6) reduced E6 expression without affecting E7. However, E7-specific siRNA (siE7) targeting both E7 open reading frame (ORF) and E6 RNA 3′-untranslated region (UTR) reduces E7 and partial E6 proteins.[23] We found that ESM1 in cervical cancer is regulated by oncogenic HPV both E6 and E7.

HPV E6 and E7 regulate gene expression directly or indirectly. Using the online prediction databases JASPR, GeneMANIA, and STRING, we found no meaningful binding sites between HPV E6 or E7 and ESM1 at both the gene and protein levels, and the underlying regulatory mechanism might be achieved through indirect means. As a group of powerful regulators, miRNAs can bind to multiple mRNAs through seed sequence complementarity and are involved in various cellular processes such as cell growth, differentiation, and apoptosis. MiRNAs have the potential to influence the replication of HPV DNA in cases of cervical cancer.[14] Conversely, the expression of multiple miRNAs is regulated by HPV oncoproteins. HPV E6 and E7 can induce the overexpression of DNA methyltransferase enzymes, which can catalyze the aberrant methylation of protein-coding and miRNA genes.[24] Based on the aberrantly expressed miRNAs in cervical cancer summarized by Tornesello et al., we intersected the downregulated (DR) miRNAs with predicted miRNAs that have complementary sequences to the ESM1 3 ′UTR region generated from miRDB (all listed miRNAs) and TargetScan (miRNAs with prediction score >90). Among the three intersecting miRNAs, miR-205-5p was significantly downregulated in both E6-and E7-expressing cells, indicating that it may mediate the regulation of ESM1 expression. The decreased expression of miR-205-5p was observed in both CIN and cancer samples compared to normal samples, which may serve as an early biomarker in the diagnosis of premalignant cervical lesions.[25] Through miR-205-5p inhibitor or mimic transfection and dual luciferase reporter assays, we confirmed that ESM1 is a target of ESM1 in cervical cancer.

To further elucidate the underlying biological function of ESM1 in CESCs, we performed functional analysis based on GO, KEGG, and GESA. The DEGs exhibited enrichment in the PI3K/Akt and MAPK signaling pathways, aligning with prior research. Both the above signaling pathways are implicated in aerobic glycolysis,[26,27] which plays a pivotal role in the metabolic regulation of cancer cells, as supported by a multitude of studies that have shown its beneficial influence on the growth, survival, proliferation, and sustained maintenance of cancer cells.[28] Though HPV E6 and E7 were demonstrated to play a role in the Akt/mTOR pathway, the specific involvement of ESM1 in aerobic glycolysis remains uncertain. By conducting bioinformatics analysis and experimental verification, we have discovered that ESM1 has the potential to influence the Akt/mTOR pathway, consequently leading to the promotion of glycolysis in cervical cancer cells. The activation of glycolysis by mTOR is achieved by modulating the expression of the transcription factor HIF-1α, which subsequently upregulates the transcription of nearly all glycolytic genes in tumor cells.[29] This mechanism potentially explains the observed changes in the expression levels of various glycolytic enzymes, as well as the significant effects on glucose consumption and lactate production, following the modulation of ESM1 expression in HeLa and SiHa cells. Our findings demonstrated that, to a certain extent, ESM1 plays a role in the activation of aerobic glycolysis via the Akt/mTOR pathway, thereby facilitating the bioenergetics and anabolic requirements for cervical cancer cell survival and proliferation.

In summary, high ESM1 expression predicts poor survival and could be considered an independent prognostic factor for cervical cancer. Elevated expression of ESM1 is regulated by HPV E6 and E7 oncoproteins by reducing miR-205-5p, which targets the 3′ untranslated region of ESM1 mRNA. Increased ESM1 expression accelerates aerobic glycolysis in cervical cancer cells through the activation of the Akt/mTOR signaling pathway. Our current work reveals the prognostic and carcinogenic roles of ESM1 in cervical cancer.

Limitations of the study

This study elucidated the significance of ESM1 in predicting the prognosis of patients with CESC and in facilitating aerobic glycolysis in cervical cancer cells. While our findings indicate that elevated ESM1 levels were triggered by oncogenic HPV E6 and E7, this was specifically demonstrated in cervical cancer cells positive for HPV 16 or 18. The regulation of ESM1 expression by other high-risk HPV types remains uncertain. In addition, it is worth conducting a more comprehensive assessment of the carcinogenic potential of ESM1 in animal models in future.

STAR★METHODS

Detailed methods are provided in the online version of this paper and include the following:

- KEY RESOURCES TABLE
- RESOURCE AVAILABILITY
  - Lead contact
  - Materials availability
  - Data and code availability
- EXPERIMENTAL MODEL AND STUDY PARTICIPANT DETAILS
  - Patient specimens
- METHOD DETAILS
  - TCGA, GTEx and GEO datasets
  - Data processing
  - Cell culture and reagents
  - RNAi and cell transfection
  - Real-time quantitative PCR, immunoblotting, and enzyme-linked immunosorbent assay
  - Luciferase reporter assay
  - Cell counting Kit-8 assay
  - Glucose uptake assay, lactate production assay and ATP production assay
- QUANTIFICATION AND STATISTICAL ANALYSIS

SUPPLEMENTAL INFORMATION

Supplemental information can be found online at https://doi.org/10.1016/j.isci.2024.110112.

ACKNOWLEDGMENTS

This study was supported by the National Natural Science Foundation of China (82002755, 82303249), Natural Science Foundation of Shandong Province (ZR2020QH206, ZR2021QH273, ZR2023QH144), Youth Innovation Team Plan in Colleges and Universities of Shandong Province (2022KJ198), and National Nature Science Foundation Cultivating Fund from the Qianfoshan Hospital of Shandong Province (QYPY2021NSFC0602, QYPYRC2022NSFC1004).

AUTHOR CONTRIBUTIONS

H.C. and C.W. conceived the study. H.C., L.Y., and Y.W. planned and designed experiments. L.Y., Y.W., M.Y., M.C., and Z.F. performed experiments. M.Y. and M.C. analyzed the computational data. H.C., L.Y., and C.W. wrote and edited the article.

DECLARATION OF INTERESTS

The authors declare that they have no competing interests.

Received: December 20, 2023
Revised: April 16, 2024
Accepted: May 23, 2024
Published: May 27, 2024

REFERENCES

1. Sung, H., Ferlay, J., Siegel, R.L., Laversanne, M., Soerjomataram, I., Jemal, A., and Bray, F. (2021). Global Cancer Statistics 2020: GLOBOCAN Estimates of Incidence and Mortality Worldwide for 36 Cancers in 185 Countries. CA. Cancer J. Clin. *71*, 209–249. https://doi.org/10.3322/caac.21660.
2. Hoppe-Seyler, K., Bossler, F., Braun, J.A., Herrmann, A.L., and Hoppe-Seyler, F. (2018). The HPV E6/E7 Oncogenes: Key Factors for Viral Carcinogenesis and Therapeutic Targets. Trends Microbiol. *26*, 158–168. https://doi.org/10.1016/j.tim.2017.07.007.
3. Yuan, Y., Cai, X., Shen, F., and Ma, F. (2021). HPV post-infection microenvironment and cervical cancer. Cancer Lett. *497*, 243–254. https://doi.org/10.1016/j.canlet.2020.10.034.
4. Shrestha, A.D., Neupane, D., Vedsted, P., and Kallestrup, P. (2018). Cervical Cancer Prevalence, Incidence and Mortality in Low

and Middle Income Countries: A Systematic Review. Asian Pac. J. Cancer Prev. *19*, 319–324. https://doi.org/10.22034/APJCP.2018.19.2.319.

5. Nalewajska, M., Gurazda, K., Marchelek-Mysliwiec, M., Pawlik, A., and Dziedziejko, V. (2020). The Role of Endocan in Selected Kidney Diseases. Int. J. Mol. Sci. *21*, 6119. https://doi.org/10.3390/ijms21176119.
6. Balta, S., Mikhailidis, D.P., Demirkol, S., Ozturk, C., Kurtoglu, E., Demir, M., Celik, T., Turker, T., and Iyisoy, A. (2014). Endocan–a novel inflammatory indicator in newly diagnosed patients with hypertension: a pilot study. Angiology *65*, 773–777. https://doi.org/10.1177/0003319713513492.
7. Afsar, B., Takir, M., Kostek, O., Covic, A., and Kanbay, M. (2014). Endocan: a new molecule playing a role in the development of hypertension and chronic kidney disease? J. Clin. Hypertens. *16*, 914–916. https://doi.org/10.1111/jch.12440.
8. Maurage, C.A., Adam, E., Minéo, J.F., Sarrazin, S., Debunne, M., Siminski, R.M., Baroncini, M., Lassalle, P., Blond, S., and Delehedde, M. (2009). Endocan expression and localization in human glioblastomas. J. Neuropathol. Exp. Neurol. *68*, 633–641. https://doi.org/10.1097/NEN.0b013e3181a52a7f.
9. De Freitas Caires, N., Gaudet, A., Portier, L., Tsicopoulos, A., Mathieu, D., and Lassalle, P. (2018). Endocan, sepsis, pneumonia, and acute respiratory distress syndrome. Crit. Care *22*, 280. https://doi.org/10.1186/s13054-018-2222-7.
10. Liu, W., Yang, Y., He, B., Ma, F., Sun, F., Guo, M., Zhang, M., and Dong, Z. (2021). ESM1 promotes triple-negative breast cancer cell proliferation through activating AKT/NF-κB/Cyclin D1 pathway. Ann. Transl. Med. *9*, 533. https://doi.org/10.21037/atm-20-7005.
11. Kang, Y.H., Ji, N.Y., Han, S.R., Lee, C.I., Kim, J.W., Yeom, Y.I., Kim, Y.H., Chun, H.K., Kim, J.W., Chung, J.W., et al. (2012). ESM-1 regulates cell growth and metastatic process through activation of NF-κB in colorectal cancer. Cell. Signal. *24*, 1940–1949. https://doi.org/10.1016/j.cellsig.2012.06.004.
12. Liu, L., Zhu, H., Wang, P., and Wu, S. (2022). Construction of a Six-Gene Prognostic Risk Model Related to Hypoxia and Angiogenesis for Cervical Cancer. Front. Genet. *13*, 923263. https://doi.org/10.3389/fgene.2022.923263.
13. Li, D., Su, X., Xue, S., Yao, L., Yu, D., Tang, X., and Huang, Y. (2023). Targeting ESM1/VEGFα signaling axis: a promising therapeutic avenue for angiogenesis in cervical squamous cell carcinoma. J. Cancer *14*, 1725–1735. https://doi.org/10.7150/jca.84654.
14. Shen, S., Zhang, S., Liu, P., Wang, J., and Du, H. (2020). Potential role of microRNAs in the treatment and diagnosis of cervical cancer. Cancer Genet. *248–249*, 25–30. https://doi.org/10.1016/j.cancergen.2020.09.003.
15. Tornesello, M.L., Faraonio, R., Buonaguro, L., Annunziata, C., Starita, N., Cerasuolo, A., Pezzuto, F., Tornesello, A.L., and Buonaguro, F.M. (2020). The Role of microRNAs, Long Non-coding RNAs, and Circular RNAs in Cervical Cancer. Front. Oncol. *10*, 150. https://doi.org/10.3389/fonc.2020.00150.
16. Lu, J., Liu, Q., Zhu, L., Liu, Y., Zhu, X., Peng, S., Chen, M., and Li, P. (2022). Endothelial cell-specific molecule 1 drives cervical cancer progression. Cell Death Dis. *13*, 1043. https://doi.org/10.1038/s41419-022-05501-5.
17. Hu, C., Liu, T., Han, C., Xuan, Y., Jiang, D., Sun, Y., Zhang, X., Zhang, W., Xu, Y., Liu, Y., et al. (2022). HPV E6/E7 promotes aerobic glycolysis in cervical cancer by regulating IGF2BP2 to stabilize m(6)A-MYC expression. Int. J. Biol. Sci. *18*, 507–521. https://doi.org/10.7150/ijbs.67770.
18. Zhang, L., Wu, J., Ling, M.T., Zhao, L., and Zhao, K.N. (2015). The role of the PI3K/Akt/mTOR signalling pathway in human cancers induced by infection with human papillomaviruses. Mol. Cancer *14*, 87. https://doi.org/10.1186/s12943-015-0361-x.
19. Cai, L., Hu, C., Yu, S., Liu, L., Yu, X., Chen, J., Liu, X., Lin, F., Zhang, C., Li, W., and Yan, X. (2020). Identification and validation of a six-gene signature associated with glycolysis to predict the prognosis of patients with cervical cancer. BMC Cancer *20*, 1133. https://doi.org/10.1186/s12885-020-07598-3.
20. Matsuo, K., Machida, H., Mandelbaum, R.S., Konishi, I., and Mikami, M. (2019). Validation of the 2018 FIGO cervical cancer staging system. Gynecol. Oncol. *152*, 87–93. https://doi.org/10.1016/j.ygyno.2018.10.026.
21. Bender, O., Gunduz, M., Cigdem, S., Hatipoglu, O.F., Acar, M., Kaya, M., Grenman, R., Gunduz, E., and Ugur, K.S. (2018). Functional analysis of ESM1 by siRNA knockdown in primary and metastatic head and neck cancer cells. J. Oral Pathol. Med. *47*, 40–47. https://doi.org/10.1111/jop.12648.
22. Huang, Y.G., Wang, Y., Zhu, R.J., Tang, K., Tang, X.B., and Su, X.M. (2021). EMS1/DLL4-Notch Signaling Axis Augments Cell Cycle-Mediated Tumorigenesis and Progress in Human Adrenocortical Carcinoma. Front. Oncol. *11*, 771579. https://doi.org/10.3389/fonc.2021.771579.
23. Tang, S., Tao, M., McCoy, J.P., Jr., and Zheng, Z.M. (2006). The E7 oncoprotein is translated from spliced E6*I transcripts in high-risk human papillomavirus type 16- or type 18-positive cervical cancer cell lines via translation reinitiation. J. Virol. *80*, 4249–4263. https://doi.org/10.1128/JVI.80.9.4249-4263.2006.
24. Jimenez-Wences, H., Peralta-Zaragoza, O., and Fernandez-Tilapa, G. (2014). Human papilloma virus, DNA methylation and microRNA expression in cervical cancer (Review). Oncol. Rep. *31*, 2467–2476. https://doi.org/10.3892/or.2014.3142.
25. Dudea-Simon, M., Mihu, D., Pop, L.A., Ciortea, R., Malutan, A.M., Diculescu, D., Ciocan, C.A., Cojocneanu, R.M., Simon, V., Bucuri, C., et al. (2022). Alteration of Gene and miRNA Expression in Cervical Intraepithelial Neoplasia and Cervical Cancer. Int. J. Mol. Sci. *23*, 6054. https://doi.org/10.3390/ijms23116054.
26. Liu, Q.P., Luo, Q., Deng, B., Ju, Y., and Song, G.B. (2020). Stiffer Matrix Accelerates Migration of Hepatocellular Carcinoma Cells through Enhanced Aerobic Glycolysis Via the MAPK-YAP Signaling. Cancers *12*, 490. https://doi.org/10.3390/cancers12020490.
27. Hu, X., Xu, Q., Wan, H., Hu, Y., Xing, S., Yang, H., Gao, Y., and He, Z. (2020). PI3K-Akt-mTOR/PFKFB3 pathway mediated lung fibroblast aerobic glycolysis and collagen synthesis in lipopolysaccharide-induced pulmonary fibrosis. Lab. Invest. *100*, 801–811. https://doi.org/10.1038/s41374-020-0404-9.
28. Liberti, M.V., and Locasale, J.W. (2016). The Warburg Effect: How Does it Benefit Cancer Cells? Trends Biochem. Sci. *41*, 211–218. https://doi.org/10.1016/j.tibs.2015.12.001.
29. Cheng, S.C., Quintin, J., Cramer, R.A., Shepardson, K.M., Saeed, S., Kumar, V., Giamarellos-Bourboulis, E.J., Martens, J.H.A., Rao, N.A., Aghajanirefah, A., et al. (2014). mTOR- and HIF-1α-mediated aerobic glycolysis as metabolic basis for trained immunity. Science *345*, 1250684. https://doi.org/10.1126/science.1250684.
30. Vivian, J., Rao, A.A., Nothaft, F.A., Ketchum, C., Armstrong, J., Novak, A., Pfeil, J., Narkizian, J., Deran, A.D., Musselman-Brown, A., et al. (2017). Toil enables reproducible, open source, big biomedical data analyses. Nat. Biotechnol. *35*, 314–316. https://doi.org/10.1038/nbt.3772.
31. Love, M.I., Huber, W., and Anders, S. (2014). Moderated estimation of fold change and dispersion for RNA-seq data with DESeq2. Genome Biol. *15*, 550. https://doi.org/10.1186/s13059-014-0550-8.
32. Yu, G., Wang, L.G., Han, Y., and He, Q.Y. (2012). clusterProfiler: an R package for comparing biological themes among gene clusters. OMICS *16*, 284–287. https://doi.org/10.1089/omi.2011.0118.
33. Liu, J., Lichtenberg, T., Hoadley, K.A., Poisson, L.M., Lazar, A.J., Cherniack, A.D., Kovatich, A.J., Benz, C.C., Levine, D.A., Lee, A.V., et al. (2018). An Integrated TCGA Pan-Cancer Clinical Data Resource to Drive High-Quality Survival Outcome Analytics. Cell *173*, 400–416.e11. https://doi.org/10.1016/j.cell.2018.02.052.
34. Chen, H., Zhang, Q., Qiao, L., Fan, X., Zhang, W., Zhao, W., and Chen, J.J. (2017). Cdc6 contributes to abrogating the G1 checkpoint under hypoxic conditions in HPV E7 expressing cells. Sci. Rep. *7*, 2927. https://doi.org/10.1038/s41598-017-03060-w.

STAR★METHODS

KEY RESOURCES TABLE

REAGENT or RESOURCE	SOURCE	IDENTIFIER
Antibodies		
Rabbit anti-ESM1	Huabio	Cat# ER62414; RRID: AB_3099428
Rabbit anti-pRb	Huabio	Cat# ET1607-9; RRID: AB_3069784
Rabbit anti-p53	Proteintech	Cat# 10442-1-AP; RRID: AB_2206609
Rabbit anti-Akt	Abways	Cat# CY5561; RRID: AB_3099435
Rabbit anti-pAkt	Abways	Cat# CY6569; RRID: AB_3099436
Rabbit anti-mTOR	Abways	Cat# CY5306; RRID: AB_3099432
Rabbit anti-pmTOR	Abways	Cat# CY6571; RRID: AB_3099434
Rabbit anti-PI3K	Abways	Cat# CY5355; RRID: AB_3099430
Rabbit anti-pPI3K	Abways	Cat# CY6427; RRID: AB_3099429
Rabbit anti-HIF1-α	Abways	Cat# CY5824; RRID: AB_3099431
Rabbit anti-β-actin	Abways	Cat# AB0035; RRID: AB_2904142
Rabbit anti-GAPDH	Huabio	Cat# ET1601-4; RRID: AB_3069615
Goat anti-Rabbit IgG	ZSGB-Bio	Cat# ZB-2301; RRID: AB_274741
Biological samples		
Cervical cancer tissues and normal control tissues	This paper	N/A
Cervical cancer serum and healthy control serum	This paper	N/A
Chemicals, peptides, and recombinant proteins		
Puromycin	SoLarbio	Cat# P8230
LY294002	MCE	Cat# HY-10108
Lipofectamine 3000	Invitrogen	Cat# L3000-015
jetPRIME	Polyplus	Cat# PT-114-15
Critical commercial assays		
Evo M-MLV RT Kit	Accurate Biology	Cat# AG11711
SYBR Green Pro Taq HS	Accurate Biology	Cat# AG11701
All-in-One miRNA qRT-PCR Detection Kit	GeneCopoeia	Cat# QP115
Cell Counting Kit-8 assay kit	APExBIO	Cat# K1018
CheKine Micro Lactate Assay Kit	Abbkine	Cat# KTB1100
CheKine Micro Glucose Assay Kit	Abbkine	Cat# KTB1300
ATP Content Assay Kit	Solarbio	Cat# BC0300
Luciferase Assay Kit	Promega	Cat# E1500
Enzyme-linked immunosorbent assay Kit	Keyybio	Cat# 51597H1
Deposited data		
Raw bulk RNAseq data	This paper	TCGA database
Affymetrix Human Genome U133A Array	This paper	GEO: GSE9750
Affymetrix Human Genome U133 Plus 2.0 Array	This paper	GEO: GSE63514
Experimental models: Cell lines		
Human: HeLa cervical cancer cells	ATCC	CCL-2
Human: SiHa cervical cancer cells	ATCC	HTB-35

(*Continued on next page*)

Continued

REAGENT or RESOURCE	SOURCE	IDENTIFIER
Human: CaSki cervical cancer cells	ATCC	CRL-1550
Human: C33A cervical cancer cells	ATCC	HTB-31
Human: Retinal pigment epithelium cell line	Laboratory of Dr. Jason J Chen	N/A
Recombinant DNA		
PCDNA3.1-ESM1	This paper	N/A
PCDNA3.1-Vector	This paper	N/A
Software and algorithms		
GraphPad Prism 8	GraphPad software, inc.	N/A
ImageJ	National Institute of Health	N/A
Xiantao bioinformatics tool	Shanghai Youlika Tec.	N/A

RESOURCE AVAILABILITY

Lead contact

Further information and request for resources should be directed to the lead contact Hanxiang Chen (hxchen@sdfmu.edu.cn).

Materials availability

Any materials generated from this study are available upon request from the corresponding authors/lead contact.

Data and code availability

- All raw bulk RNAseq data we used in this research are available in the TCGA and the GEO databases, which are publicly available.
- This paper does not report original code.
- All other additional information and raw data are available from the lead contact upon request.

EXPERIMENTAL MODEL AND STUDY PARTICIPANT DETAILS

Patient specimens

A total of 39 non-cancer cervical tissue samples and 69 cervical cancer tissue samples were obtained from Shandong First Medical University & Shandong Provincial Qianfoshan Hospital for the purpose of conducting RT-qPCR and Immunoblotting analysis. Additionally, 52 healthy serum samples and 116 cervical cancer serum samples were collected from the same institution for the purpose of performing ELISA assay. All cervical tissues were confirmed by pathological analysis and stored in liquid nitrogen before RNA extraction and protein extraction. This study was approved by the Ethics Committee of Shandong Provincial Qianfoshan Hospital, and conducted in accordance with the Helsinki Declaration.

METHOD DETAILS

TCGA, GTEx and GEO datasets

Clinical information and gene expression quantification data for CESC patients were downloaded from TCGA dataset. Gene expression data with clinical information on healthy cervical tissues were acquired from the Genotype-Tissue Expression (GTEx) database. Gene expression levels were determined using the UCSC Xena Toil RNA-seq pipeline.[30] A total of 306 cervical cancer samples and 13 healthy cervix controls were enrolled in this study. GSE9750 (with 24 normal cervical tissues and 33 cervical cancer tissues) and GSE63514 (with 24 normal cervical tissues, 14 CIN1 tissues, 22 CIN2 tissues, 40 CIN3 tissues, and 28 cervical cancer tissues) from the Gene Expression Omnibus (GEO) database were used as the validation datasets.

Data processing

The R programming language (version 3.6.3) was the principal tool used for analyzing the data throughout the study. Differentially expressed genes between cervical cancer samples and healthy controls with different clinical stages were identified using the DESeq2 package (version1.26.0).[31] Gene ontology (GO), Kyoto Encyclopedia of Genes and Genomes (KEGG) and GSEA analysis were conducted using the clusterProfiler package (version 3.14.3),[32] and visualized using the ggplot2 package (version 3.3.3). Survival analysis and survival curves were generated using the Survminer package (version 0.4.9). The survival pROC package (version 1.17.0.1) was used to create the ROC curve. Nomogram and calibration analysis were performed using the rms package (version 6.2–0) and the survival package (version 3.2–10).[33]

Cell culture and reagents

The cervical cancer cell lines HeLa, SiHa, CaSki, C33A, and the normal cervix-derived cell line H8, as well as the human embryonic kidney 293T (HEK293T) cells, were procured from the American Type Culture Collection (ATCC) and maintained in Dulbecco's modified Eagle's medium (DMEM, Gibco, USA) supplemented with 10% fetal bovine serum (FBS, Gibco, USA). The human retinal pigment epithelium cell line (RPE1) was maintained in a 1:1 dilution of DMEM-Ham's F-12 medium with 10% NBS. RPE1 cells stably expressing pBabe or HPV-16 E6/E7 were established by retrovirus-mediated infection using a pBabe-puro-based retroviral construct. Cells were selected using 10.5 μg/mL puromycin for 3–6 days, maintained at a concentration of 6.5 μg/mL and used within 15 passages. Cells were maintained in culture at low passage numbers and consistently passaged using Trypsin-EDTA 0.25% (Invitrogen, USA). Regular testing for mycoplasma contamination was conducted, with all cells used for experiments confirmed to be mycoplasma negative at the time of testing. The PI3K/Akt signaling pathway inhibitor LY294002 was used at a concentration of 20 μM.

RNAi and cell transfection

Specific small interfering RNAs (siRNAs) targeting ESM1, HPV 16E6 (si209), 16E7 (si198), HPV 18E6 (si219), 18E7 (si220),[23] and negative control siRNA (siNC) were purchased from Ruibo (China). miR-205-5p mimics/inhibitor were synthesized by GenePharma (China). The pENTER-hESM1 and control plasmids utilized in the overexpression experiments were constructed by Wzbio (China). Cell transfection was performed at a concentration of 60 nM for miRNA mimics, 120 nM for miRNA inhibitor, and 20 nM for siRNA using Lipofectamine 3000 transfection reagents according to the manufacturer's instructions (Invitrogen, USA). Cell transfection with plasmids was performed at an amount of 2 μg using jetPRime reagent (Polyplus transfection, Ozyme) according to the manufacturer's instructions. The oligo sequences are shown in Table S1.

Real-time quantitative PCR, immunoblotting, and enzyme-linked immunosorbent assay

Real-time quantitative PCR (RT-qPCR) and immunoblotting were performed according to the manufacturer's instructions.[34] All primers were synthesized by BioSune (China) and the primer sequences are listed in Table S1. The following primary antibodies were used: ESM1 (1:1000; Huabio, China), pRb (1:1000; Huabio, China), p53 (1:2000; Proteintech, China), Akt (1:1000, Abways, China), *p*-Akt (1:1000, Abways, China), mTOR (1:1000, Abways, China), *p*-mTOR (1:1000, Abways, China), PI3K (1:1000, Abways, China), p-PI3K (1:500, Abways, China), HIF-1α (1:1000, Abways, China), β-actin (1:5000, Abways, China) and GAPDH (1:5000, Huabio, China). The secondary antibody used was goat anti-rabbit (1:10000, ZSGB-Bio, China).

The ESM1 expression levels in serum were detected by Enzyme-linked immunosorbent assay (ELISA) according to the instruction of ELISA kit which was purchased from Keyybio (China).

Luciferase reporter assay

The 3′-UTR sequence of ESM1, containing three putative miR-205-5p binding sites, was cloned into the pmirGLO miRNA target expression vector (Promega, USA). Plasmids with mutant predictive miR-205-5p binding sites were constructed by BioSune (China). miR-205-5p mimics or NC and plasmids were co-transfected into HEK293T cells using Lipofectamine 3000, according to the manufacturer's instructions. Firefly and Renilla luciferase activities were detected using the dual-luciferase reporter system (Promega, USA) 48 h after transfection. Firefly luciferase activity was normalized to the Renilla luciferase activity.

Cell counting Kit-8 assay

The transduced cells were seeded into 96-well plates at a density of 2×10^3 cells/well and cultured for 24, 48, 72, and 96 h. Subsequently, 10 μL of the CCK-8 solution (APExBIO, USA) was added to each well. After incubation for 2 h at 37°C, the optical density was measured using a Multiskan GO microplate reader (ThermoFisher, USA) at 450 nm.

Glucose uptake assay, lactate production assay and ATP production assay

The transfected cells were seeded into 6-well plates at a density of 2×10^5 cells per well. Culture medium was collected after incubation for 48 h at 37°C. Glucose and lactate levels in the culture medium were detected using the CheKine Glucose Assay Kit (Abbkine, China) and CheKine Lactate Assay Kit (Abbkine, China), respectively, according to the manufacturer's protocol.

ATP Assay Kit (Solarbio, China) was used to measure cellular ATP contents according to the manufacturer's protocol. Briefly, cell lysate and ATP reaction buffer was mixed and incubated for 30 min. Absorbance was measured by OD at 660 nm wavelength.

QUANTIFICATION AND STATISTICAL ANALYSIS

The R programming language and GraphPad Prism software (version 7.0) were used for statistical analysis. Univariate and multivariate Cox regression analysis were performed to evaluate the prognostic value of ESM1 in CESC. Kaplan-Meier curves were used to assess differences in overall survival, progression-free interval, and disease-specific survival between the high-risk and low-risk score groups, and the significance was determined by the log rank test. Hazard ratios (HR) and 95% confidence intervals (CI) were calculated to evaluate variables associated with overall survival. One-way analysis of variance (ANOVA) or two-tailed Student's t-tests were used to calculate significant differences. The gray value of the protein was determined using ImageJ software. $p < 0.05$ was used as a cutoff value for significance.